Self-regulatory Enzyme-actuated Macroscale Patterning of ATP-loaded Nanoparticle

Ekta Shandilya [a], *Subhabrata Maiti** [a]

[a]Department of Chemical Sciences, Indian Institute of Science Education and Research (IISER) Mohali, Knowledge City, Manauli 140306 (India).

*Corresponding author

Subhabrata Maiti

E-mail: smaiti@iisermohali.ac.in

ORCID - 0000-0002-2554-0762

ABSTRACT

Directional interactions and assembly of nanobioconjugate in clusters at specific location are important for patterning, microarrays to biomedical research. Herein, we report self-assembly and spatial control in surface patterning of the surfactant-functionalized nanoparticles can be governed in macroscale environment by two factors – synergistic enzyme-substrate-nanoparticle affinity and phoretic effect. Firstly, we showed aggregation of cationic gold nanoparticle (GNP) can be modulated by multivalent anionic nanoparticle binding adenosine-based nucleotide and enzyme, alkaline phosphatase. We further demonstrated two different types of their autonomous aggregation pattern – (i) by introducing enzyme gradient which modulates the synergistic non-equilibrium interactivity of the nanoparticle, nucleotide and enzyme in macroscale and (ii) surface deposition pattern from evaporating droplet via coffee ring effect. Finally, we showed change in capillary phoresis parameters responsible for coffee ring due to introduction of ATP-loaded GNP in blood serum, showing immense applicability in low-cost disease diagnostics. Overall, a unique method for macroscale surface nanobiopatterning has been demonstrated having potential application in controlled large area patterning with diverse cascade catalytic surface and spatiotemporal multisensory-based application.

KEYWORDS

Multivalent interaction • Nanoparticle assembly • Enzyme • Nucleotides • Coffee Ring effect • Capillary phoresis • Spatiotemporal biosensors

TABLE OF CONTENTS

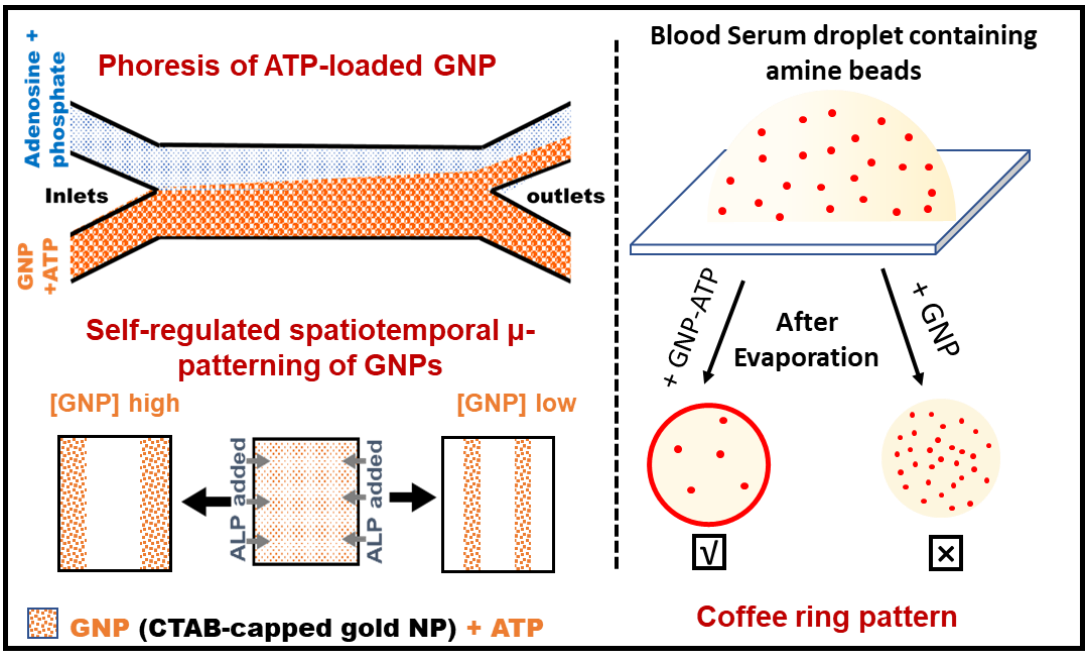

INTRODUCTION

Gaining control over surface patterning in both micro- and macroscale regime is a demanding technology for its applicability in designing task-specific materials and devices for optoelectronics, plasmonic to (bio)analysis and catalysis.[1-3] However, for proper precision and periodicity of the patterning, one has to rely on techniques like various kind of lithography, such as – optical, electron or ion beam, contact printing, soft lithography using masked deposition etc.[4-7] Although these are very efficient surface patterning strategy, the certain disadvantages are – pre-treatment or post-treatment of the surface; costly in nature; instead of being autonomous, skilled operation is necessary for proper outcome.[8] Recently, researchers are employing molecular and supramolecular self-assembly strategy over a surface for autonomous and versatile surface-patterning which are cost-effective in various analysis purposes and applicable for large area patterning also.[8-13] It is worthy to mention that biological world used competitive and dynamic self-assembly process for spatiotemporal patterning which are automated and governed by the local microscale interactivity.[9,14-16]

Commonly, surface immobilized enzyme, specific protein-ligand binding affinity, complementary DNA strand or DNA origami-driven nanoparticle organization or pH- or light responsive molecular assembly etc. have been known for gradient and localized patterning by utilizing both non-template and template-assisted strategy.[17-20] Herein, we used affinity between specific enzyme, alkaline phosphatase (ALP) and its adenosine nucleotide-based substrates, namely – adenosine mono/di/triphosphate (AM/D/TP) which are non-covalently bound to a

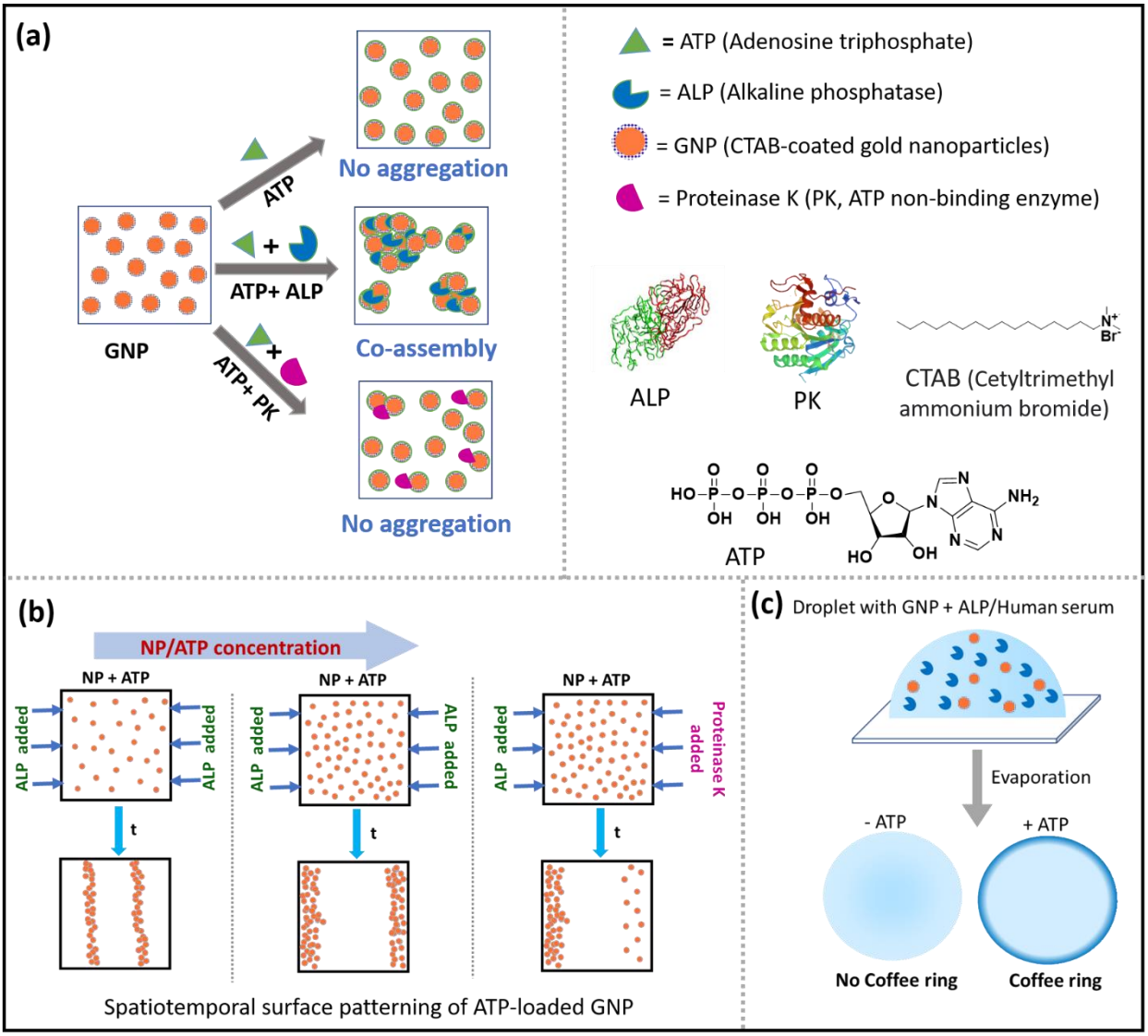

Fig. 1. Schematic representation showing a) specific aggregation of GNP in simultaneous presence of ATP and ALP; b) spatial aggregation pattern in gradient of ALP and c) coffee ring effect upon evaporation of droplet due to evaporation of droplet containing blood serum with GNP-ATP conjugate.

nanoparticle surface to prompt assembly of the overall ensemble in a spatiotemporally controllable way in a gradient of enzymes and from evaporating droplets. The unique features and advantages of this strategy are – (i) synergistic interactivity leads coexisted assembly and

patterning of both nanoparticles and enzymes in a millimeter scale region of a glass slide by diffusiophoretic process, (ii) modulation of coffee ring pattern (generated due to evaporation of the colloidal droplet on a glass surface) by the presence of specific ATP-loaded nanoparticle with both interactive and non-interactive enzymes and finally, (iii) translation of this effect in a drying blood serum droplet which can have applicability in low-cost on spot disease diagnostics. It is worthy to mention here, enzyme-substrate interactivity driven colloidal chemotaxis-cum-phoresis behavior including coffee ring phenomenon are one of the important areas among contemporary nanobiotechnology owing to their applicability in both fundamental understanding of the biomolecular phoresis and their application in forensics to diagnostics assays.[21-26]

Here, at first, we showed cationic surfactant-bound gold nanoparticle (GNP) surface sequester anionic nucleotide (adenosine mono/di/triphosphate (AMP/ADP/ATP) which simultaneously undergo aggregation in presence of the specific presence of enzymes, ALP (Fig. 1a). Subsequently, we showed the spatial localization of the GNP/ATP/ALP aggregating zone can be patterned by selective enzyme-substrate gradient (Fig. 1b). Finally coffee ring formation pattern from an evaporating droplets solution of aqueous buffer and blood serum due the presence of specific GNP-ATP conjugate has been explored (Fig. 1c).

RESULTS AND DISCUSSION

Numerous self-assembly and patterning processes in biological systems, ranging from cell-cell adhesion to metabolon formation to viral infection are governed by multivalent interactions.[27-32] This has inspired chemists and physicists to develop experimental synthetic systems that recreate

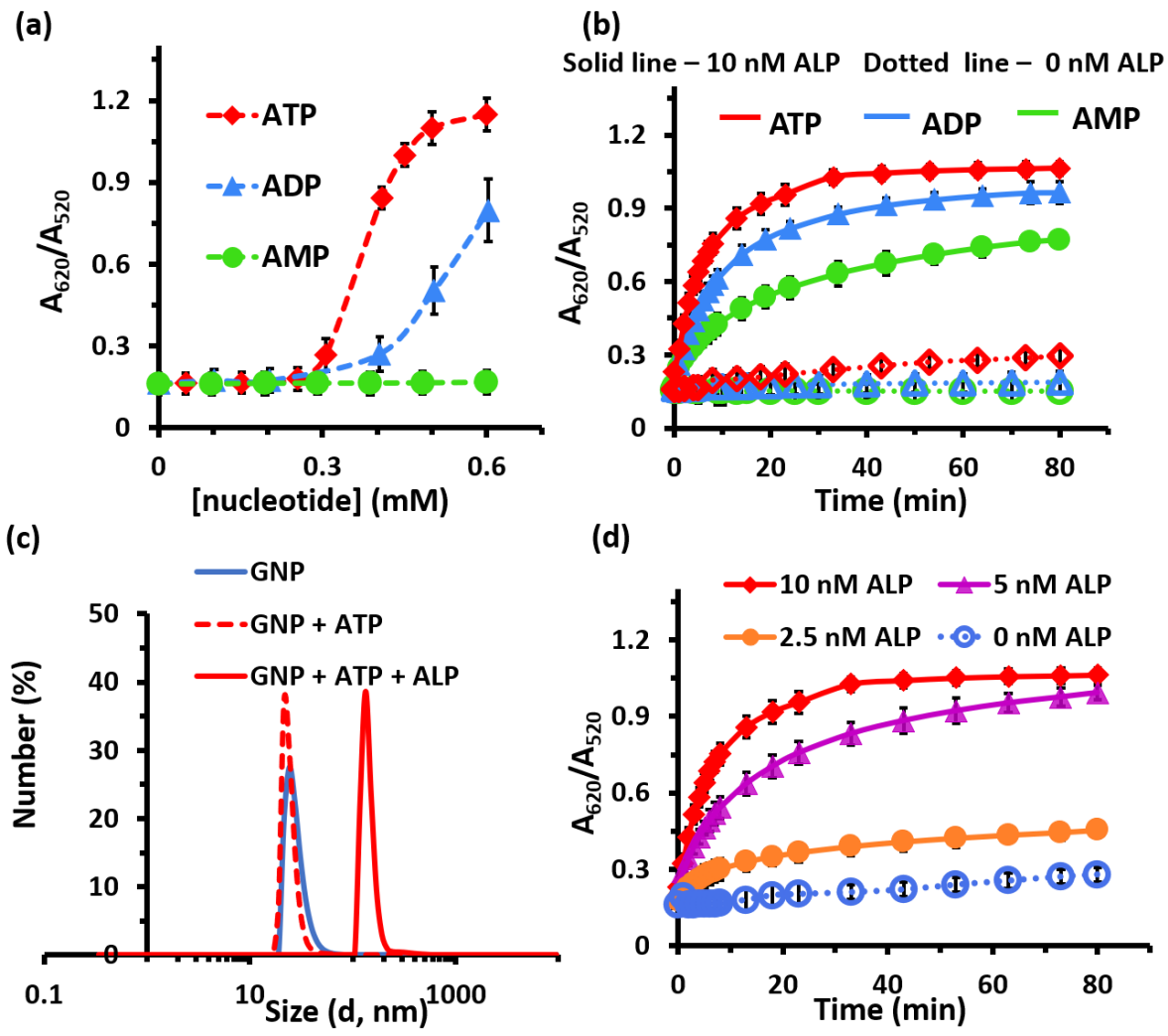

Fig. 2. (a) Change in UV-vis absorbance ratio at 620 and 520 nm (A620/A520) ratio of CTAB-capped GNP in presence of different concentration of AMP, ADP and ATP (0-0.6 mM). (b) Change in A_{620}/A_{520} ratio in absence (dotted line) and presence (solid line) of fixed concentration of alkaline phosphatase (ALP = 10 nM) with time having keeping fixed concentration of AMP or ADP or ATP (0.3 mM). (c) Hydrodynamic diameter (Dh) of the GNP in absence and presence of only ATP and ATP+ALP after 60 min of their mixing. [ATP] = 0.3 mM, [ALP] = 10 nM (d) Change in UV-vis absorbance ratio (A620/A520) of GNP as a function of time in presence of fixed concentration of ATP (0.3 mM), but different concentration of ALP (0-10 nM). [Tris] = 15 mM, pH = 9.

life-like dynamicity.[33-38] The multivalent interactive properties of nucleotides like- adenosine triphosphate (ATP) have been used to trigger formation of self-assembled structures, like - vesicles or to initiate signal transduction and catalytic processes from a nanoparticle surface.[39-41] Inspired by these results, here at first, we decided to explore the interaction and effectivity of multiple charge counter-ions with a charged nanoparticle surface in inducing their aggregation. For this, we synthesized cetyltrimethyl ammonium bromide (CTAB)-capped gold nanoparticles (GNP) (having positive surface charge) using the previously reported procedure (details in Supporting Information (SI)). The synthesized GNP had characteristic surface plasmon resonance absorption at 525 nm and diameter around 22 ± 3 nm (Fig. S1, supporting information (SI)). Next, we chose adenosine-based nucleotides such as adenosine triphosphate (ATP), adenosine diphosphate (ADP), and adenosine monophosphate (AMP) to observe the multivalent binding effect and corresponding assembly of cationic GNP. The aggregation behavior of the nanoparticles was followed using UV-vis spectroscopy by following the ratio of absorbance peak at 620 and 520 nm (A_{620}/A_{520}). It is worthy to mention that this ratio has been used in the literature for the quantification of the extent of GNP aggregation as the sharp surface plasmon of GNP at 520 nm gets broadened while aggregating, thus A_{520} gets decreased with an increase at A_{620}.[42] The aggregation behavior was studied by fixing GNP concentration at 120 pM ([Au] = 100 μM), and nucleotides were then titrated in it with increasing concentration. In each case, the values were recorded up to 1 h after their mixing. We observed that the rate of increasing A_{620}/A_{520} value follows the trend of ATP>ADP>AMP, suggesting the role of multiple charged interaction in triggering assembly (Fig. 2a, S2, SI). In particular, aggregation of GNP started prominently after the addition of 0.35 and 0.45 mM of ATP and ADP respectively, (at 0.3 mM and 0.4 mM of ATP

and ADP, it is sufficiently stable) whereas almost no aggregation was observed in case of AMP, even after adding 0.6 mM of it. We also confirmed this by dynamic light scattering (DLS), where a similar trend was observed (Fig. S9, SI). Residence of nucleotides on the GNP surface was confirmed by zeta (ζ) potential measurement, with a ζ -value for CTAB-capped cationic GNP of 40 ± 2 mV, which decreased to 20 ± 4, 30 ± 3, 35 ± 2 and 34 ± 3 mV in presence of 0.3 mM of ATP, ADP, AMP and adenosine + Pi, respectively in our experimental condition (Fig. S11, SI). This data also suggests that the residential propensity and affinity of multiple phosphate towards cationic surface is stronger than for single phosphate. We also determined the concentration of nucleotides bound on the GNP surface by using ultracentrifugation dialysis method as shown in Fig. S3, SI. In presence of fixed 0.3 mM of ATP/ADP/AMP, the amount of ATP, ADP and AMP bound on the GNP surface are 0.26, 0.18 and 0.08 mM, respectively.

In situ reversible assembly-disassembly processes of a surfactant or nanoparticle-based systems governed by multivalent interactions have been previously reported, where the number of multivalent bonds is simply decreased by physicochemical processes, triggered by enzymes or light.[45] Many dynamic assembly processes with attractive features like programmed reactors or delivery vehicles have been reported where surfactant assembly was triggered by ATP and their corresponding dissociation to AMP or adenosine + inorganic phosphate (3Pi) by using enzymes like ATPase or phosphatase.[33-34] In our case, we also expected to observe no additional assembly of the GNP by introducing the enzyme ALP in the system, as ALP is known to dissociate ATP to adenosine + 3 Pi. To this end, we monitored aggregation kinetics by following A_{620}/A_{520} ratio over course of 80 minutes in 15 mM tris-HCl buffer, pH 9 at 25 °C. To our surprise, we observed

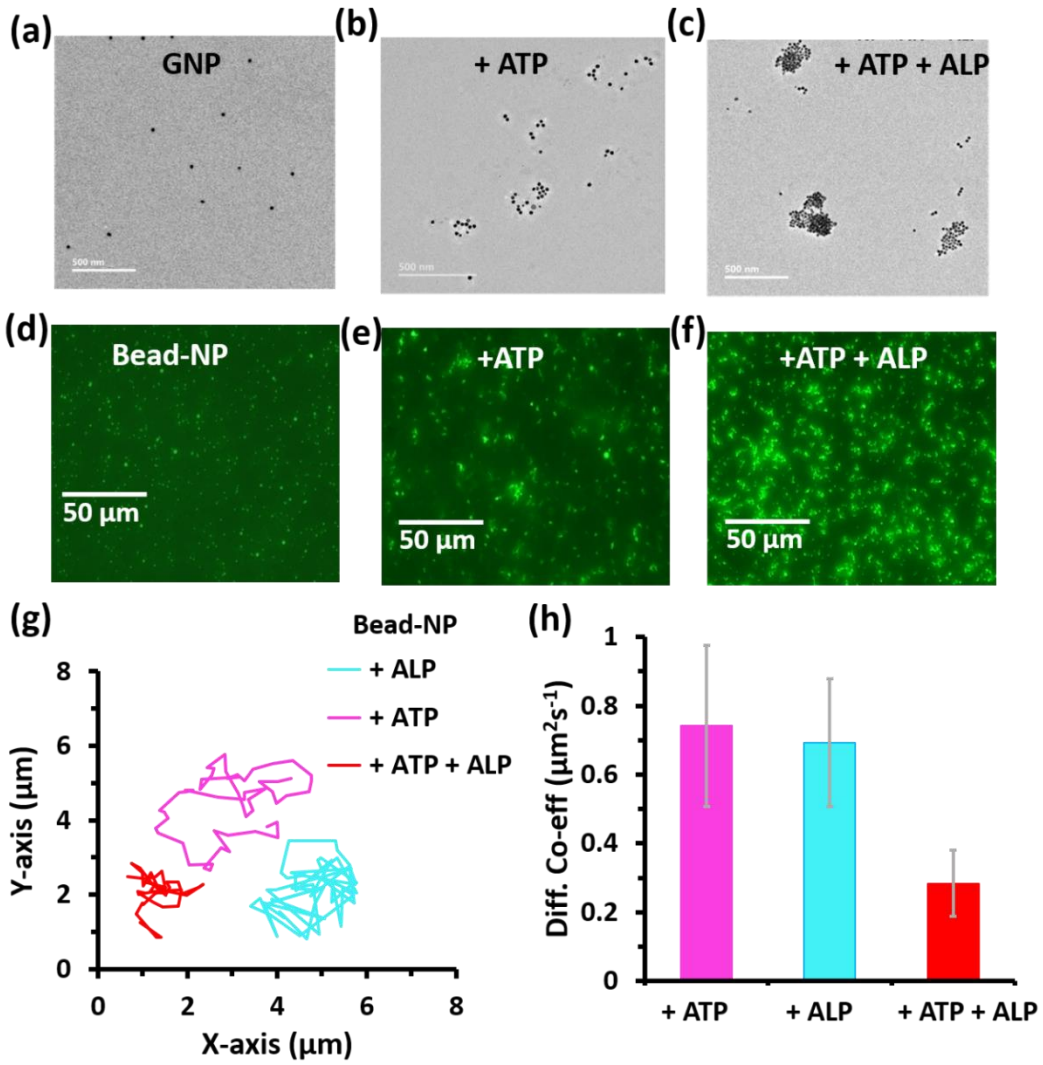

Fig. 3. TEM images of (a) only GNP, (b) GNP + ATP (0.3 mM), (c) GNP + ALP (10 nM) + ATP (0.3 mM) after 60 min of mixing. Fluorescence microscopic images of fluorescent polystyrene bead-NP conjugate (d) without ATP and ALP, (e) with only ATP (0.3 mM) (f) with ATP (0.3 mM) and ALP (10 nM) after 60 min of mixing. (g) Trajectory of Bead-NP conjugate in presence of ATP (0.3 mM), ALP (10 nM) and (ATP+ALP) over 10 sec in the XY plane observed under optical microscope and analyzed using Tracker software. (b) Diffusion co-efficient of Bead-NP conjugate in those systems as obtained from the slope of the MSD curves using MSD=4DΔt. 10 Bead-NP conjugates from 5 sets of experiment has been taken for analysis.

much higher aggregation rate of the GNP in presence of enzyme, rather than full disassembly or decreased aggregation. It is to be noted here that using only enzyme (0-10 nM) in the absence of ATP and in presence of only ATP (0-0.3 mM) without ALP did not trigger any notable aggregation of the nanoparticle system (Fig. 2b-c, S4+S7, SI). Moreover, GNP aggregation was observed in simultaneous presence of ADP (0.3 mM) + ALP or AMP (0.3 mM) + ALP (Fig. 1b, S4-S6, SI). We also noted higher rate of aggregation by ALP in the presence of ATP compared to ADP and AMP (Fig. 2b, SI). These observations were confirmed by DLS (dynamic light scattering) measurements. The average size observed for ATP, ADP, and AMP was 735 ± 60 nm, 540 ± 30 nm, and 410 ± 22 nm in the presence of ALP, while 117 ± 17 nm, 62 ± 3 nm, and 52 ± 10 nm were measured in the absence of ALP, in all those cases, 60 minutes after addition (Fig. S10, SI). Next, we measured aggregation while varying ALP and keeping ATP concentration (0.3 mM) fixed. Interestingly, we observed an increase in both A_{620}/A_{520} and size values, suggesting an increase in the extent of aggregation with increasing ALP concentration (Fig. 2d, S4-S6+S9, SI). Transmission electron microscopy (TEM) images further corroborated our observations (Fig. 3a-c). We also checked this using GNP-tagged fluorescent bead (~2 μm diameter), which also showed higher aggregation only in presence of ATP and ALP, observed clearly from the fluorescence microscope images (Fig. 3d-f, Fig. S21, SI). By tracking their diffusion, the diffusion of the bead in presence of ATP and ALP together is almost 2.5 times lower than in presence of only ALP and ATP with the bead separately, suggesting larger aggregated structures (Fig. 3g-h, S22, SI). Overall, the extent and rate of aggregation of the nanoparticle can be controlled by – (i) fixing ALP concentration and varying the amount of ATP, (ii) fixing ATP concentration and varying the

amount of ALP and (iii) fixing enzyme concentration, by varying the extent of multivalent interaction i.e. by changing ATP, ADP or AMP at a particular concentration.

After observing the GNP aggregation phenomenon only in simultaneous presence of ATP, including other nucleotides (ADP and AMP) and ALP, we were curious to explore some in depth insights of this process. At first, we checked the zeta potential of the system. Interestingly, the zeta potential decreased to 10 ± 2 mV in simultaneous presence of ALP (10 nM) and ATP (0.3 mM) at our experimental condition after 1 h. We also checked the zeta potential of GNP in presence of AMP and ADP in presence of ALP in two separate experiments. We found in each case, zeta potential value decreases to below 20 mV and the rate of decrease in zeta potential with time follows the order: ATP > ADP> AMP (Fig. S12, SI). It suggests that probably presence of nucleotides on the surface of GNP also made the enzyme resides on the nanoparticle surface and the extent of aggregation with ALP is higher in presence of strongly-bound nucleotides. As ALP is a negatively charged enzyme with zeta value of -30 ± 5 mV, it destabilizes the colloidal stability of the cationic GNP surface more as it acts or binds on the surface of the cationic nanoparticle, specifically due to the presence of its substrate, resulting aggregation.[43-44]

Herein, we also checked the hydrolyzing ability of ALP over these nucleotide phosphates in absence and presence of GNP. For this we performed HPLC experiment and measured the amount adenosine formed after 60 min of the reaction. Here, we checked the hydrolysis for AMP, ADP and ATP under same experimental condition. In each case, 0.3 mM of nucleotides were used as substrates of ALP. We found almost similar concentration of free adenosine formed (~33 % cleavage) with AMP, both in absence (0.10 ± 0.01 mM) and presence of GNP (0.098 ± 0.015 mM) in the system, suggesting presence of GNP did not significantly alter the rate of the reaction. In case of ADP, the amount of formed adenosine (~15 % cleavage) decreased than AMP and were

found to be 0.041 ± 0.003 mM and 0.038 ± 0.002 mM in absence and presence of NP, respectively. However, in presence of ATP, strikingly the formed amount of adenosine (~6 % cleavage) were 0.021± 0.002 and 0.016 ± 0.002 mM, in absence and presence of GNP respectively (Fig. S18-S20, SI). It suggests that there is a sharp decrease in hydrolytic rate of ATP in presence of GNP, compared to other two. It is important to note that ALP hydrolyzed efficiently to monophosphoester in comparison to di- and triphosphosphoester, which also reflected in their hydrolytic ability towards AMP, ADP and ATP, although the binding affinity is almost comparable in each cases.[46-47] In fact, ALP is also known to bind with the product phosphates which can act as a competitive inhibitor.[46] As mentioned before, ALP also possesses the ability to bind with the product phosphates at a micromolar level binding affinity. We also checked the effect of the nucleotide-hydrolyzed product adenosine (0.3 mM) and phosphates (0.9 mM) in generating aggregation process (Fig. S8, SI). In fact, in this case, we also observed aggregation of GNP upon addition of ALP and the aggregation kinetics is much lower than ATP, but comparable to AMP. We believe this is due to the lower binding affinity of phosphates with GNP compared to ATP. Overall, in our system, as the hydrolyzed product was also capable of aggregate formation, hence, we were not able to observe any disassembly behavior of the GNP, at our experimental condition. These data indicate the following facts: (i) the hydrolysis of nucleotides by ALP is far from been completed after 1 h, although in that time interval almost complete aggregation and precipitation happened. (ii) The aggregation is higher with nucleotides having stronger binding affinity to the nanoparticle but lower hydrolyzing ability with the ALP. It is to be noted here, in our experimental condition, surface nature and concentration regime of the nanoparticle, nucleotides and reaction condition are different from other reported literature where presence of ALP helped to generate a transient assembly of nanoparticles.[48]

After analyzing the above results, we were also curious to perform few other control experiments to check the enzyme-substrate selectivity in GNP aggregation. For this we selected an anionic multivalent peptide substrate, tetraaspartate (DDDD) and checked the binding affinity on GNP surface. Upon titrating, we found at 0.2 mM concentration of DDDD, the GNP remains stable and after that it started to aggregate. Now, we were pleased to observe that in a stable mixture of 0.2 mM of DDDD and GNP, addition of ALP (10 nM) does not result any aggregation, under similar experimental condition (Fig. S14, SI). Next, we checked if we used a protease enzyme for which DDDD can act as the substrates and for that we have chosen proteinase K (PK) which is a non-specific peptidase.[49] In fact, we observed upon addition of enzyme, PK in the mixture of GNP+DDDD, a slightly faster aggregation happens, suggesting simultaneous and synergistic interactivity of all three components, GNP, substrate and substrate-specific enzyme are necessary for aggregation to occur at this experimental condition. The aggregation is much lesser than GNP-ATP-ALP system, as the zeta potential of PK is -8 ± 2 mV in comparison to zeta potential of ALP which is -28 ± 3 mV in our experimental condition (pH = 9, Tris buffer). In fact, we also did not observe any additional decrease in zeta potential of GNP-DDDD system upon introduction of PK, unlike ALP in GNP-ATP/ADP/AMP (Fig. S12, SI). Additionally, we checked instead of using ALP, if PK can induce GNP-ATP conjugate aggregation in presence of ALP but no notable aggregation was observed (Fig. S15-S16, SI). We also checked instead of using phosphate, if carbonate solution can induce GNP aggregation in presence of ALP (Fig. S17, SI). Here again we did not observe any GNP aggregation as carbonate as anion does not have any affinity to the enzyme, ALP, but only to GNP-surface; supporting our hypothesis of synergistic interactivity.

These results further made us interested in controlling aggregation pattern in a macroscale system by introducing gradient of enzyme and GNP-ATP. For this, at first, here we performed an experiment on a glass slide by placing 15 µl of GNP-ATP ([GNP] = 120 pM, [ATP] = 0 - 0.3 mM) and placed a 2.2 cm square-shaped cover slip on it. Now from two opposite ends, we added 7 µl of FITC-ALP solution to generate a gradient of enzyme inside the coverslip as shown in Fig. 4a + Fig. S23, SI. FITC-tagging of ALP has been done just to make the aggregation pattern visible under microscope. Subsequently, we monitored the formation of fluorescent clusters across the coverslip under a microscope in five different zones A-E as designated in Fig. 4a. Interestingly, here the fluorescent structures formed only at the edge of the cover slip (i.e. at zone A and E) where FITC-ALP were added (Fig. 4b+c, S24+S25, SI) only in presence of GNP-ATP. In a control experiment, without ATP but only with GNP, we did not observe any fluorescent structure (Fig. S26, SI). The agglomeration of fluorescent clusters at zone A and E is maximum when 0.3 mM of ATP was used. In presence of 0.1 mM ATP, the tendency of formation of clusters is lower, whereas for 0.2 mM, it is formed at zone A+E as well as some structures was also observed at zone B+D, but at a much lower extent (Fig. S27, SI). Interestingly, when we performed experiments with 0.1 mM ATP and 40 pM GNP, upon addition of ALP from both sides clusters specifically formed in zone B and Zone D (Fig. S28-29, SI). We also performed additional control experiment using GNP+DDDD conjugate and gradient of ALP, which did not result any notable clustering across the coverslip (Fig. S30, SI). Upon introducing FITC-PK (FITC tagged proteinase K) gradient in GNP+ATP solution no

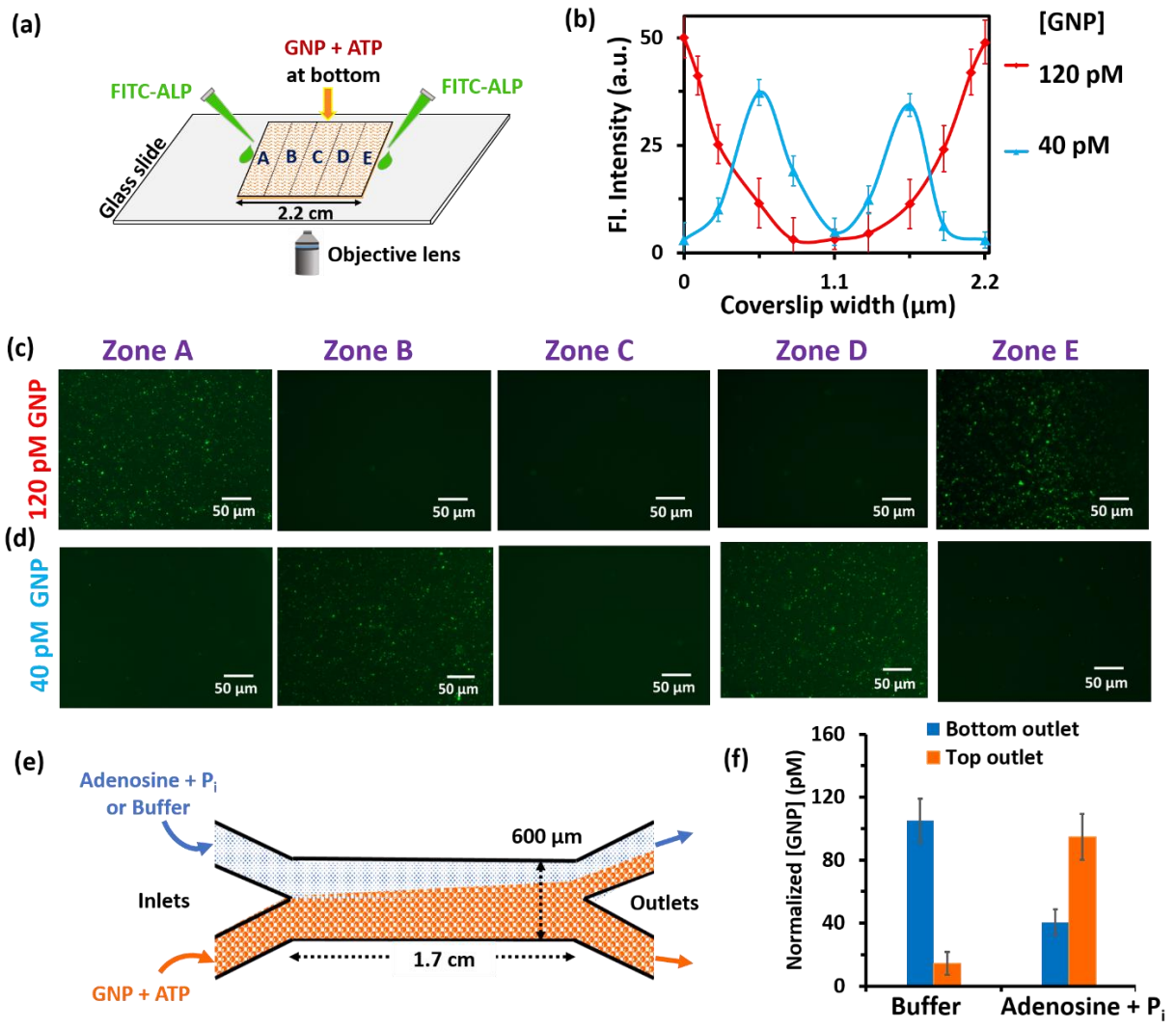

Fig. 4. (a) Schematic representation of the experimental set up where GNP (40 or 120 pM) +ATP (0.3 mM) (15 µl volume) solution was placed a glass slide and a cover slip was placed over it. Then from two sides of the cover slip, FITC-tagged ALP was added (0.5 µM, 7 µl) was added and at different time interval images were taken at zone A to E. (b) Fluorescence intensity profile across zone A to E at 10, 20 and 30 min when under the cover slip [GNP] = 120 pM and [ATP] = 0.3 mM and [GNP] = 40 pM and [ATP] = 0.1 mM. (c-d) Representative fluorescent image showing agglomeration of the fluorescent structure in different zone in presence of 120 and 40 pM of GNP after 30 minutes of reaction. (e) Schematic of the 2-inlet-2-outlet microfluidic set up used in our

experiment where from the top inlet adenosine+Pi solution or buffer and through bottom inlet, GNP+ATP solution were injected at a total flow rate of 320 μl/h. (f) Normalized concentration of GNP eluted through top and bottom outlet when buffer or adenosine + Pi were passed through top inlet and GNP+ATP through bottom. Experimental condition: [Ade] = 0.3 mM, [Pi] = 0.9 mM, [ATP] = 0.3 mM, [GNP] = 120 pM, [tris] = 15 mM, pH = 9.

formation of clusters was observed (Fig. S28, SI). However, with RITC-PK gradient in GNP+DDDD solution, a much lower concentration of cluster was observed at zone A and E (Fig. S31-S33, SI). This experiment also indicated requirement of synergistic interactivity among GNP, substrate and enzyme for the formation of patterned clustering.

We reasoned this process is due to diffusiophoretic migration (combined effect of both electrophoresis and chemiphoresis) of positively charged GNP-ATP conjugate to negative charge enzyme.[50-54] We theoretically verified the electrophoretic migration using COMSOL multiphysics software (for details see Fig. S35-S37 and related discussion in SI). The chemiphoretic part in this case resulted due to hydrolysis of ATP near the ALP to create adenosine and three phosphate molecules, thereby creating a solute gradient of high to low concentration across the nanoparticle surface (Fig. S37, SI). We also experimentally probed this effect in a 2-inlet-2-outlet microfluidic channel as detailed in Fig. 4d+e, S34, SI. Here through one inlet, we injected GNP+ATP conjugate and through other inlet Ade+Pi and in control experiment only buffer. After analyzing the amount of GNP passed through both the outlet, we found that GNP-ATP conjugate drifted more to adenosine+Pi side by more than 5-fold compared to buffer, suggesting possible chemiphoretic effect in this case. It is to be noted here diffusiophoresis-mediated formation of spatially controlled colloidal aggregates or bands in gradient of salts has been reported in previous literature also.[55-57]

However, in our case we have generated this gradient enzymatically, where gradient of enzyme result dissociation of ATP to adenosine and Pi in a selective zone, resulting concentration gradient in the system. Here for stronger chemiphoretic and electrophoretic contribution at higher GNP and ATP concentration, clustering was observed at terminal zone (A and E); whereas for weaker chemiphoresis and electrophoresis at lower GNP and ATP concentration, clustering was observed at inner B and D zone.

Subsequently, we also wanted to investigate how this GNP-ATP-ALP interaction and aggregation phenomenon affect the 'coffee ring' phenomenon of an evaporating droplet. Usually coffee-ring formation is due to the deposition of suspended or dispersed materials particularly on the edge of the droplet after complete evaporation of the liquid.[58-61] Here, net outward capillary flow from the center of the droplet to edge generates as the liquid from the edge of the droplet evaporates faster than center. Nonetheless, the formation and suppression of coffee ring phenomenon are a matter of interest due to their immense applicability in surface coating, printing to bioanalysis.[24-26,58-61] Until now, this has mostly been investigated with nanoparticles of different sizes and shape, surfactants or with biomolecules, cells etc. However, the presence of simultaneous interactivity among the particulate matters (GNP, enzyme) and small molecule (ATP) in a droplet might alter the pattern. In fact, this strategy can be translated as a low-cost biosensor in complex biofluids, like blood serum to identify the presence of ATP-bound enzyme.

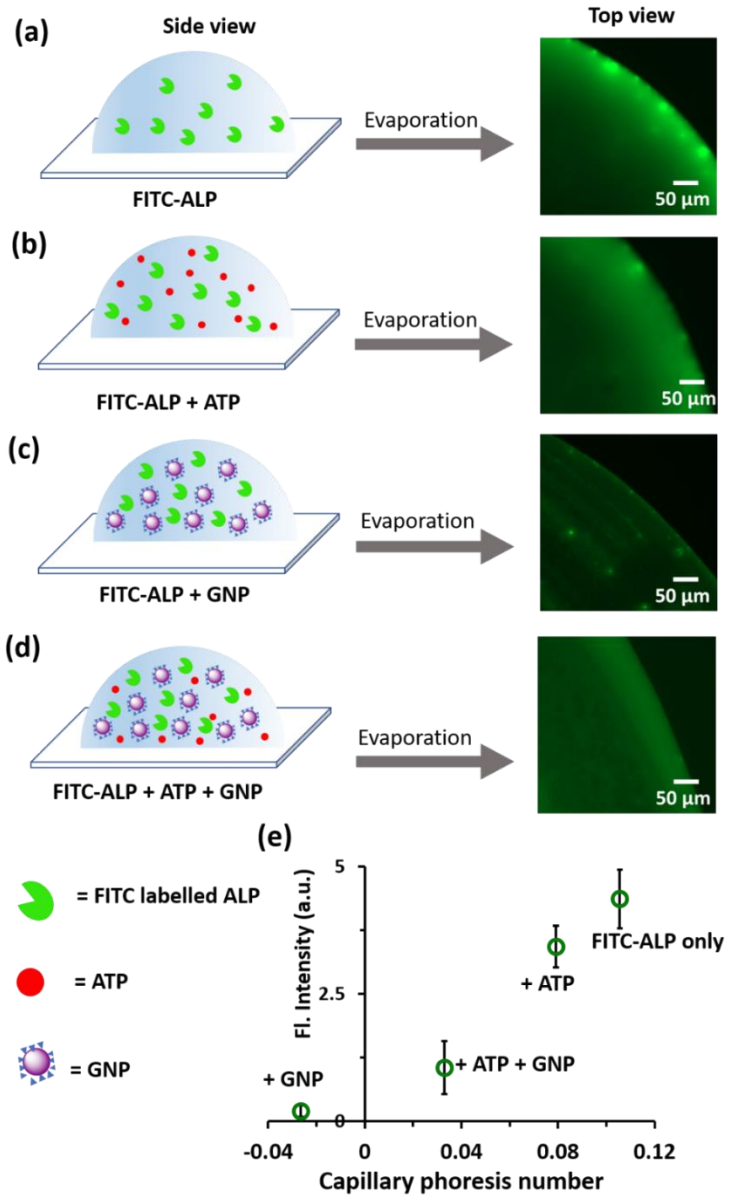

Fig. **5.** Fluorescence microscopic images of the spatiotemporal pattern of the ring-like structure formation after the evaporation of a droplet consisting of FITC-ALP uniformly mixed with (a) only buffer, b) buffer + ATP, c) buffer + GNP, d) buffer + GNP + ATP. Experimental conditions: [GNP] = 120 pM, [ATP] = 0.3 mM, [FITC-ALP] = 500 nM, [Tris] = 15 mM, pH = 9. e) Correlation between coffee ring intensity and capillary phoresis number. Fluorescence intensity of the image was calculated using imageJ software and for details about CP value calculation, please see SI.

As mentioned in the preceding paragraph, to understand the coffee ring effect of GNP-ATP-ALP conjugate, we first tagged ALP with FITC and followed the deposition of the enzyme under fluorescence microscope due to evaporation of droplet of 1 µl volume of tris-buffer solution (pH = 9) in a glass slide (Fig. 5). In presence of only buffer and ATP, it formed clear ring like deposition at the periphery of the droplet. Interestingly, in presence of GNP in the buffer, ring width becomes significantly lower and FITC-ALP deposited almost throughout the droplet surface. Now, while following the deposition pattern in presence of GNP+ATP+ALP, we observed much thicker ring width. The ring pattern formation probability and its extent of formation can be explained by calculating the electrokinetics driven capillary phoresis (CP) number, as higher the CP value, higher is the propensity of coffee ring formation and vice-versa.[61] CP number is dictated by diffusiophoretic velocity arise due to salt buffer gradient upon evaporation, diffusioosmosis driven fluid transport along the surface and capillary convection within the droplet (Fig. S38, please see SI for detailed calculation). The highest CP value was observed for only enzyme system and lowest for GNP based system and hence the trend in coffee ring width was observed. Interestingly, here although simultaneous presence of ALP and ATP result aggregates which, in principle, can suppress the coffee ring pattern even more than only GNP + ALP system, but we observed slightly higher due to the higher electrokinetic effect due to the decrease in net positive charge of the overall conjugate and thus experienced less frictional force from the negatively charged glass surface (Table S1, SI). Trend in CP value also corroborate with fluorescence intensity of the ring (Fig. 5e, Table S1, SI)

The above-mentioned observation prompted us to investigate the coffee ring pattern formation behavior in a much complex biological fluid, blood serum. This system does not simply consist

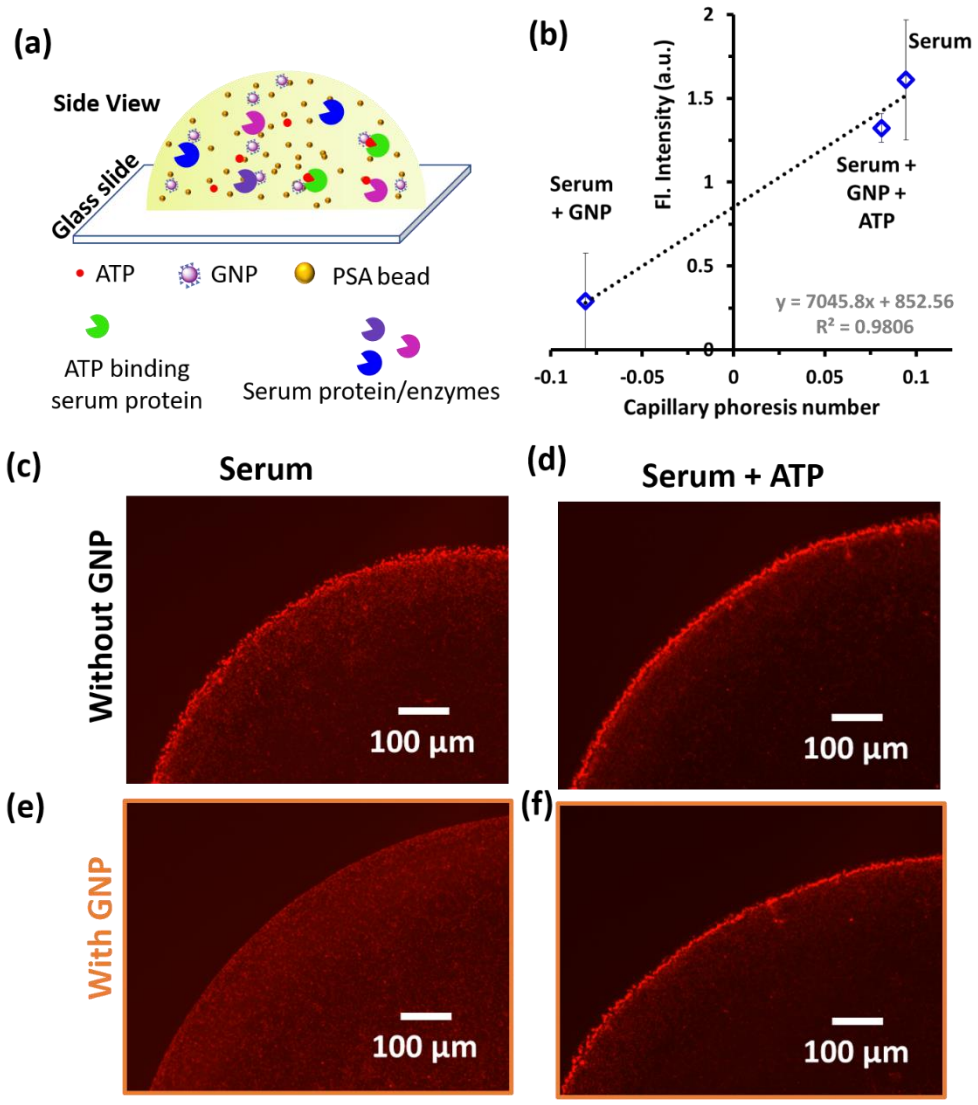

Fig. 6. (a) Schematic representation showing human blood serum droplet with GNP, ATP, ALP together and vice-versa. (b) Correlation between coffee ring intensity and capillary phoresis number. (c-f) Fluorescence microscopic images of the spatiotemporal pattern of the ring-like structure formation after the evaporation of a serum droplet consisting of GNP, ATP and GNP+ATP. Fluorescence intensity of the image was calculated using imageJ software and for details about CP value calculation, please see SI.

of buffer, rather with numerous proteins (like albumin, α/β/γ-globulin), enzymes, salts and small molecules.[62] Herein, we used a diluted (0.1%) serum solution in pH = 9 Tris buffer for both ζ-

potential measurement and coffee ring pattern formation. ζ-potential value of only serum was found to be -28 mV, corroborating presence of mostly negative charged proteins, like albumin (50-60%), α/β-globulin (30-40%) (among globulin proteins, γ-globulin is positive charge in neutral condition with a pI of 7.2, which is only ~10% content in the serum, among proteins or enzymes). In fact, we also checked that our commercially procured blood serum solution showed phosphoesterase like activity (Fig. S39, SI) confirming presence of ATPase. Now to understand the coffee ring formation pattern of serum in absence and presence of GNP or ATP, we used commercial negatively charged polystyrene amine (PSA) fluorescence bead (0.025 wt%, ζ- value = -30 mV, diameter ~1 μm) to follow the deposition pattern from an evaporating droplet in a glass slide, as mentioned in the earlier paragraph (Fig. 6a). In presence of only serum and serum+ATP, we observed clear coffee ring formation as the beads deposited on the edge of the droplet. In presence of GNP only in blood serum, we did not observe clear coffee ring like deposition of the fluorescent beads. The suppression of coffee ring effect in presence of only GNP is due to its high positive zeta potential (25 ± 2 mV) even in presence of negatively charged blood serum containing proteins. This actually results net negative CP value due to stronger inward directed diffusiophoretic flow as the zeta of glass surface also becomes 31 ± 2. In a way, it also suggests that only GNP does not attract proteins on its surface from blood serum in our experimental condition. Interestingly, again simply by adding GNP+ATP conjugate, the net positive ζ-value decreased significantly to 4 ± 2 mV in blood serum (Fig. 6b). It suggests serum binding protein/enzymes gets attracted to the GNP-ATP surface. Moreover, we were pleased to observe the restoration of coffee ring pattern due to suppression of inward diffusiophoretic flow with higher CP value (Fig. 6g, Table S1, SI). Thus, modulation of capillary phoresis by GNP-ATP conjugate can be used as a sensor in identifying ATP-binding protein (like heat shock protein (HSP90)) or

phosphatase-like enzyme in complex environment like blood serum, simply through observation of phoresis-mediated surface pattern formation on a glass slide.[63]

Conclusion

In conclusion, this work amalgamated both non-covalently bound GNP-substrate conjugate and enzyme in one platform demonstrating three phenomenon – (i) how aggregation of nanoparticle takes place in presence of nucleotide and alkaline phosphatase in homogeneous condition and (ii) how this aggregation can get patterned in macroscale over a glass slide and (iii) coffee ring pattern from an evaporating droplet, also applicable in clinically relevant sample, blood serum. In fact, our finding demonstrates here diffusiophoretic effect dictates the taxis and thereby assembly zone which can be actuated by introduction of the enzyme. In previous instances, many non-equilibrium and dynamic self-assembly and patterning of nanoparticles or active colloidal matter were exemplified using complementary charge interaction, light or in combination of lithography and self-assembly approach.[64-69] In fact, all of which have significant applicability in designing plasmonic or SERS-active substrates and dynamic non-linear oscillatory and catalytic systems or materials.[70-72] Here, nanoparticle together with enzyme gives access to use the pattern for catalytic surface as well as biosensors. Specifically, the ability of using GNP-ATP conjugate in modulating coffee ring formation pattern in blood serum sample to identify the content of ATP binding protein/enzyme in serum indicates the translatory ability of this pattern formation approach in clinically relevant diagnostics. Overall, this opens future research in examining complex assembly pattern of a mixed systems comprising heterogeneous nanoparticle monolayer or liposome-based systems with combinatorial enzyme-substrate reactivity.

METHODS

Synthesis of gold nanoparticles (GNPs)

Gold nanoparticles were synthesized by following previously reported protocol.[36] Briefly, 5 mL of seed solution was prepared by adding 0.25 mM of HAuCl4.4H2O to a vial containing 75 mM CTAB, followed by addition of 6 mM ice-cold freshly prepared sodium borohydride solution which resulted in formation of brown colored solution indicating formation of gold seeds. For growth solution, 1.03 mL of 24 mM of $HAuCl_4.4H_2O$ solution was added to a vial containing 5.22 mL of water, followed by addition of 10 mL of 0.1 M CTAB solution which turned the solution from light yellow to orange. After that, 7.5 mL of 0.1 M L-ascorbic acid was added to growth solution with gentle shaking, which turned the solution colorless. Finally, 62.5 μL of two hours aged seed solution was added to growth solution and blended vigorously for 20 seconds, with the appearance of red color. At last, thus formed solution was left undisturbed for 24 hours at 25 ° C and was characterized before use.

Aggregation kinetics

To understand the aggregation of GNP in presence of different nucleotides (ATP/ADP/AMP), peptide (D-D-D-D), enzymes (alkaline phosphatase, proteinase K), and salts (phosphate and carbonate) UV-vis spectroscopic measurements were followed using Agilent Cary 60 spectrophotometer. For which 10 mm quartz cuvette procured from Optiglass. In most of the cases, 120 pM nanoparticle concentration was used and reaction volume was fixed to 1 mL. Further, to ensure aggregation, DLS (dynamic light scattering) studies and zeta potential measurements were carried out for same samples using Horiba zetasizer SZ100-V2.

Transmission Electron Microscopy (TEM) imaging

To visualize agglomeration in NP system, JEOL JEM-F200 microscope was used. For preparing TEM samples, 120 pM were used in presence of ATP (0.3 mM), ALP (10 nM) or both. After 1 hour of incubation, around 5 - 7 μl sample was casted on TEM grid and dried under vacuum before imaging.

Diffusion co-efficient calculation

For understanding, effect of aggregation on diffusion of nanoparticles we did mean square displacement (MSD) measurements. Initially, micro-sized replica of nanoparticles (Bead-NP) was formed using carboxylate modified polystyrene bead (diameter = 2 μm) following reported protocols.[S2] For measuring MSD, sample solutions were poured into a hybridization chamber (pasted on glass slide) and sealed. The motion of these micron-sized particles was recorded at the height 200-250 μm from base of hybridization chamber during 60 seconds at a rate of 10 frames per second by using Zeiss axio observer 7 microscopes with 100x objective and AxioCam 503 Mono 3 Megapixel camera. Each recorded video was then analyzed using Tracker, a Video Analysis and Modeling Tool, which allowed the extraction of trajectories. From these trajectories, average MSD was plotted against Δt, further diffusion coefficient was calculated using $MSD = 4D\Delta t$ for every mentioned sample.

Microfluidics measurements

To understand the migratory behavior of nanoparticle in response to adenosine and phosphate which are product of ALP activity over ATP. We used a two-inlet two-outlet microfluidics chip as shown in Fig. 4d of main manuscript. 120 pM GNP solution in buffer was injected from bottom

inlet, and buffer or 0.3 mM adenosine + 0.9 mM Pi (product of 0.3 mM ATP) in 15 mM tris-HCl, pH 9 buffer was injected from top inlet at 320 µl /hr flow rate using a syringe pump (World Precision Instruments). Then after, 30 minutes of run time solution from both outlets was collected and measured using UV spectrophotometer.

Spatiotemporal patterning of nanoparticles over glass surface

For visualizing spatiotemporal patterning of NP assembly formation over glass surface, alkaline phosphatase (ALP) was labelled with FITC and proteinase K was labelled with RITC using previously reported protocols.[47] For performing experiments, 15 µl of GNP (120 pM) (with or without substrates like ATP or DDDD) was casted over glass slide, and a square coverslip (2.2 cm x 2.2 cm) was placed over it. This coverslip was divided into five zones (named from A to E) in order to interpret data. Now, from opposite edges 7 µl of enzyme solution (ALP or Proteinase K (PK)) was added and images were taken in different zones over time using 20x objective. For analysis of pictorial data, ImageJ software was used and pixel intensity (labeled as Fl. Intensity) was plotted against coverslip width.

Coffee ring pattern formation

Sample containing FITC labelled ALP (0.5 µM, 50 % labelled) was prepared with and without ATP, and also with GNP. 1 µl of this sample was drop casted over glass slide. After air drying this sample, microscopic images were taken and analyzed using ImageJ software. Similarly, for observing coffee ring formation ability of GNP in presence of blood serum, samples ith blood serum (0.1%) and 0.025 % amine functionalized beads were prepared and analyzed, and the coffee

ring intensity was plotted against capillary phoresis number (CP). The calculations for CP are given in section L of the supporting information.

ASSOCIATED CONTENT

Additional data and discussion for UV, DLS, HPLC, microfluidic measurements, fluorescence images, CP number calculation, details for theoretical study are given in supporting information file (PDF).

ACKNOWLEDGMENT

E.S. acknowledges CSIR, India (09/947(0109)/2019-EMR-I) for doctoral research grant and S.M. acknowledges Science and Engineering Research Board (SERB) (File No. SRG/2019/000365) for financial support and MHRD-STARS grant (File no. STARS/APR2019/CS/284/FS) for HPLC instrument which has been used in this study. We thank I-STEM facility for providing access to COMSOL Multiphysics 5.6.

REFERENCES

(1) C. Kim, P. E. Burrows and S. R. Forrest, *Science*, 2000, **288**, 831–833.

(2) A. G. L. Olive, N. H. Abdullah, I. Ziemecka, E. Mendes, R. Eelkema and J. H. van Esch, *Angew. Chem. Int. Ed.* 2014, **53**, 4132-4136.

(3) T. Heinrich, C. H.-H. Traulsen, M. Holzweber, S. Richter, V. Kunz, S. K. Kastner, S. O. Krabbenborg, J. Huskens, W. E. S. Unger and C. A. Schalley, *J. Am. Chem. Soc.*, 2015, **137**, 4382–4390.

(4) H. Xu and J. Huskens, *Chem -Eur. J.* 2010, **16**, 2342–2348.

(5) W. T. S. Huck, *Angew. Chem. Int. Ed.* 2007, **46,** 2754–2757.

(6) C. M. Kolodziej and H. D. Maynard, *Chem. Mater.* 2012, **24**, 774–780.

(7) G. M. Whitesides, E. Ostuni, S. Takayama, X. Jiang and D. E. Ingber, *Annu. Rev. Biomed. Eng.*, 2001, **3**, 335–373.

(8) H.-N. Barad, H. Kwon, M. Alarcón-Correa and P. Fischer, *ACS Nano*, 2021, **15**, 5861–5875.

(9) D. Pini and A. Parola, *Soft Matter*, 2017, **13**, 9259–9272.

(10) M. Zhu, G. Baffou, N. Meyerbröker and J. Polleux, *ACS Nano*, 2012, **6**, 7227–7233.

(11) D. Dorokhin, S.-H. Hsu, N. Tomczak, D. N. Reinhoudt, J. Huskens, A. H. Velders and G. J. Vancso, *ACS Nano*, 2010, **4**, 137–142.

(12) O. Roling, K. De Bruycker, B. Vonhören, L. Stricker, M. Körsgen, H. F. Arlinghaus, B. J. Ravoo and F. E. Du Prez, *Angew. Chem. Int. Ed.* 2015, **54**, 13126–13129.

(13) R. Klajn, T. P. Gray, P. J. Wesson, B. D. Myers, V. P. Dravid, S. K. Smoukov and B. A. Grzybowski,. *Adv. Funct. Mater.* 2008, **18**, 2763–2769.

(14) S. Loescher and A. Walther, *Small*, 2021, **17**, e2005668.

(15) A. J. Koch and H. Meinhardt, *Rev. Mod. Phys.* 1994, **66**, 1481–1507.

(16) P. K. Maini, T. E. Woolley, R. E. Baker, E. A. Gaffney and S. S. Lee, *Interface Focus* 2012, **2**, 487–496.

(17) X. Jiang, Q. Xu, S. K. W. Dertinger, A. D. Stroock, T.-M. Fu and G. M. Whitesides, *Anal. Chem.* 2005, **77**, 2338–2347.

(18) M. Shelly, S.-I. Lee, G. Suarato, Y. Meng and S. Pautot, *Methods Mol. Biol.*, 2017, **1493**, 321–343.

(19) P. J. Dorsey, M. Rubanov, W. Wang and R. Schulman, *ACS Macro Lett.*, 2019, **8**, 1133–1140.

(20) R. R. Mahato, Priyanka, E. Shandilya, and S. Maiti, *Chem. Sci.* 2022, **13**, 8557–8566.

(21) F. Mohajerani, X. Zhao, A. Somasundar, D. Velegol and A. Sen, *Biochemistry*, 2018, **57**, 6256–6263.

(22) J. Agudo-Canalejo, T. Adeleke-Larodo, P. Illien and R. Golestanian, *Acc. Chem. Res.*, 2018, **51**, 2365–2372.

(23) J. Li and F. Lin, *Trends Cell Biol.*, 2011, **21**, 489–497.

(24) D. Mampallil and H. B. Eral, *Adv. Colloid Interface Sci.*, 2018, **252**, 38–54.

(25) H. Li, D. Buesen, R. Williams, J. Henig, S. Stapf, K. Mukherjee, E. Freier, W. Lubitz, M. Winkler, T. Happe and N. Plumeré, *Chem. Sci.*, 2018, **9**, 7596–7605.

(26) M. Anyfantakis and D. Baigl, *Angew. Chem. Int. Ed.*, 2014, **53**, 14077–14081.

(27) E. Shandilya and S. Maiti, *ChemSystemsChem* 2020, **2**, e201900040.

(28) J. Huskens, *Curr. Opin. Chem. Biol.* 2006, **10**, 537–543.

(29) Priyanka, E. Shandilya, S. K. Brar, R. R. Mahato and S. Maiti, *Chem. Sci.*, 2021, **13**, 274–282.

(30) N. J. Overeem, P. H. E. Hamming, M. Tieke, E. van der Vries and J. Huskens, *ACS Nano*, 2021, **15**, 8525–8536.

(31) J. Huskens, L. J. Prins, R. Haag and B. J. Ravoo, *Multivalency: Concepts, Research and Applications,* John Wiley & Sons, Nashville, TN, 2018.

(32) J. M. Belitsky, A. Nelson, J. D. Hernandez, L. G. Baum and J. F. Stoddart, *Chem. Biol.*, 2007, **14**, 1140–1151.

(33) R. D. Astumian, *Nat. Commun.*, 2019, **10**, 3837.

(34) A. Sharko, D. Livitz, S. De Piccoli, K. J. M. Bishop and T. M. Hermans, *Chem. Rev.*, 2022, **122**, 11759–11777.

(35) S. Maiti, I. Fortunati, C. Ferrante, P. Scrimin and L. J. Prins, *Nat. Chem.* 2016, **8**, 725–731.

(36) R. R. Mahato, E. Shandilya, B. Dasgupta and S. Maiti, *ACS Catal.*, 2021, **11**, 8504–8509.

(37) A. Mishra, S. Dhiman and S. J. George, *Angew. Chem. Int. Ed.* 2021, **60**, 2740-2756.

(38) A. Jain, S. Dhiman, A. Dhayani, P. K. Vemula and S. J. George, *Nat. Commun.*, 2019, **10**, 450.

(39) R. K. Grötsch, C. Wanzke, M. Speckbacher, A. Angı, B. Rieger and J. Boekhoven, *J. Am. Chem. Soc.*, 2019, **141**, 9872–9878.

(40) C. Pezzato and L. J. Prins, *Nat. Commun.*, 2015, **6**, 7790.

(41) M. Weißenfels, J. Gemen and R. Klajn, *Chem*, 2021, **7**, 23–37.

(42) H. Wei, B. Li, J. Li, E. Wang and S. Dong, *Chem. Commun.* 2007, **36**, 3735–3737.

(43) M. Grzelczak, L. M. Liz-Marzán and R. Klajn, *Chem. Soc. Rev.*, 2019, **48**, 1342–1361.

(44) S. Dhiman, A. Jain, M. Kumar and S. J. George, *J. Am. Chem. Soc.*, 2017, **139**, 16568–16575.

(45) B. A. Grzybowski and W. T. S. Huck, *Nat. Nanotechnol.*, 2016, **11**, 585–592.

(46) M. L. Applebury, B. P. Johnson and J. E. Coleman, *J. Biol. Chem.*, 1970, **245**, 4968–4975.

(47) A. Deshwal and S. Maiti, *Langmuir*, 2021, **37**, 7273–7284.

(48) T. Bian, A. Gardin, J. Gemen, L. Houben, C. Perego, B. Lee, N. Elad, Z. Chu, G. M. Pavan and R. Klajn, *Nat. Chem.*, 2021, **13**, 940–949.

(49) E. V. Petrotchenko, J. J. Serpa, D. B. Hardie, M. Berjanskii, B. P. Suriyamongkol, D. S. Wishart and C. H. Borchers, *Mol. Cell. Proteomics*, 2012, **11**, M111.013524-1-M111.013524-13.

(50) D. Velegol, A. Garg, R. Guha, A. Kar and M. Kumar, *Soft Matter*, 2016, **12**, 4686–4703.

(51) J. Anderson, *Annu. Rev. Fluid Mech.*, 1989, **21**, 61–99.

(52) J. T. Ault, P. B. Warren, S. Shin and H. A. Stone, *Soft Matter*, 2017, **13**, 9015–9023.

(53) J. Palacci, B. Abécassis, C. Cottin-Bizonne, C. Ybert and L. Bocquet, *Phys. Rev. Lett.*, 2010, **104**, 138302.

(54) S. Shim, *Chem. Rev.*, 2022, **122**, 6986–7009.

(55) B. Abécassis, C. Cottin-Bizonne, C. Ybert, A. Ajdari and L. Bocquet, *Nat. Mater.*, 2008, **7**, 785–789.

(56) P. O. Staffeld and J. A. Quinn, *J. Colloid Interface Sci.*, 1989, **130**, 69–87.

(57) B. Ramm, A. Goychuk, A. Khmelinskaia, P. Blumhardt, H. Eto, K. A. Ganzinger, E. Frey and P. Schwille, *Nat. Phys.*, 2021, **17**, 850–858.

(58) R. Guha, F. Mohajerani, A. Mukhopadhyay, M. D. Collins, A. Sen and D. Velegol, *ACS Appl. Mater. Interfaces*, 2017, **9**, 43352–43362.

(59) Shikha, E. Shandilya, Priyanka, S. Maiti, *Chem. Commun.* **2022**, *58*, 9353–9356.

(60) R. D. Deegan, O. Bakajin, T. F. Dupont, G. Huber, S. R. Nagel and T. A. Witten, *Nature*, 1997, **389**, 827–829.

(61) H. Hu and R. G. Larson, *J. Phys. Chem. B*, 2006, **110**, 7090–7094.

(62) M. Leeman, J. Choi, S. Hansson, M. U. Storm and L. Nilsson, *Anal. Bioanal. Chem.*, 2018, **410**, 4867–4873.

(63) C. Garnier, D. Lafitte, P. O. Tsvetkov, P. Barbier, J. Leclerc-Devin, J.-M. Millot, C. Briand, A. A. Makarov, M. G. Catelli and V. Peyrot, *J. Biol. Chem.*, 2002, **277**, 12208–12214.

(64) C. T. Zhang, Y. Liu, X. Wang, X. Wang, S. Kolle, A. C. Balazs and J. Aizenberg, *Soft Matter*, 2020, **16**, 1463–1472.

(65) I. Lagzi, B. Kowalczyk and B. A. Grzybowski, *J. Am. Chem. Soc.*, 2010, **132**, 58–60.

(66) A. van der Weijden, M. Winkens, S. M. C. Schoenmakers, W. T. S. Huck and P. A. Korevaar, *Nat. Commun.*, 2020, **11**, 4800.

(67) W. Wang, W. Duan, S. Ahmed, A. Sen and T. E. Mallouk, *Acc. Chem. Res.*, 2015, **48**, 1938–1946.

(68) D. P. Singh, U. Choudhury, P. Fischer and A. G. Mark, *Adv. Mater.*, 2017, **29**, 1701328.

(69) X. Chen, N. Gianneschi, D. Ginger, J.-M. Nam and H. Zhang, *Adv. Mater.*, 2021, **33**, e2107344.

(70) C. Matricardi, C. Hanske, J. L. Garcia-Pomar, J. Langer, A. Mihi and L. M. Liz-Marzán, *ACS Nano*, 2018, **12**, 8531–8539.

(71) J. Deng and A. Walther, *Adv. Mater.*, 2020, **32**, e2002629.

(72) J. Leira-Iglesias, A. Tassoni, T. Adachi, M. Stich and T. M. Hermans, *Nat. Nanotechnol.*, 2018, **13**, 1021–1027.